ULTRASOUND NEWS

October 2025

Comments and illustrations of the EFSUMB guidelines. Parasitic diseases of the lungs and pleura.

Kathleen Möller[1], Christoph F. Dietrich[2]

[1]Medical Department I/Gastroenterology; SANA Hospital Lichtenberg, Berlin, Germany, [2]Department General Internal Medicine (DAIM), Hospitals Hirslanden Bern Beau Site, Salem and Permanence, Bern, Switzerland

Abstract

Parasitic infections of the lungs and pleura are uncommon but clinically significant, affecting both endemic and non-endemic areas due to global travel and migration. While computed tomography (CT) remains the imaging modality of choice, thoracic ultrasound, particularly in peripheral and pleural lesions, offers a valuable, non-invasive complement. Beyond its traditional role in detecting effusions or consolidations, ultrasound now includes advanced techniques such as contrast-enhanced ultrasound (CEUS), which enhances lesion characterization. This review summarizes the most relevant pulmonary and pleural parasitic diseases, emphasizing their characteristic findings in B-mode and CEUS, and illustrates their diagnostic importance through selected clinical cases.

Keywords: parasitosis; lung; pleura; ultrasound; CEUS

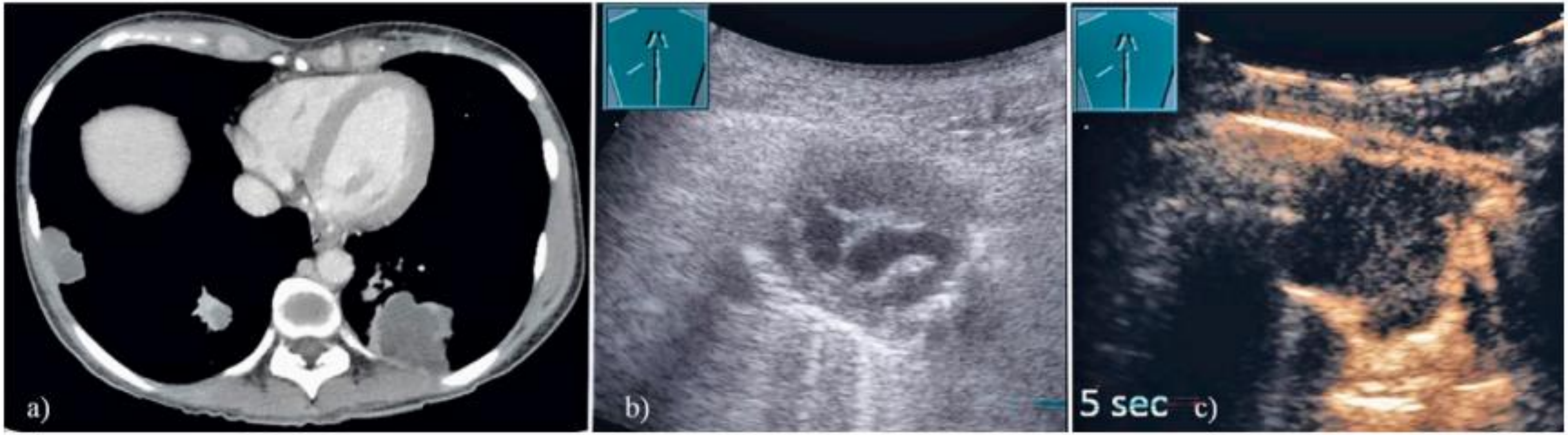

Fig 1. A 41-year-old female patient with confirmed echinococcosis cysticus with visualization of pulmonary lesions on CT (a). There are several lesions in both lungs. The largest lesion is located on the left dorsal side and is adjacent to the thoracic wall. Since there is no interposition due to lung artifacts, the lesion can be visualized in B-mode ultrasound. It is thick-walled and has equally thick-walled internal septa. However, the layering of the wall and septa cannot be clearly delineated (b). CEUS shows a lack of enhancement of the lesion. However, the enhancement of the peripheral areas is already detectable after 5 seconds, so that a pulmonary arterial enhancement can be assumed in the surrounding area (c) [courtesy Prof. Görg and Prof. Mahnken, University of Marburg].

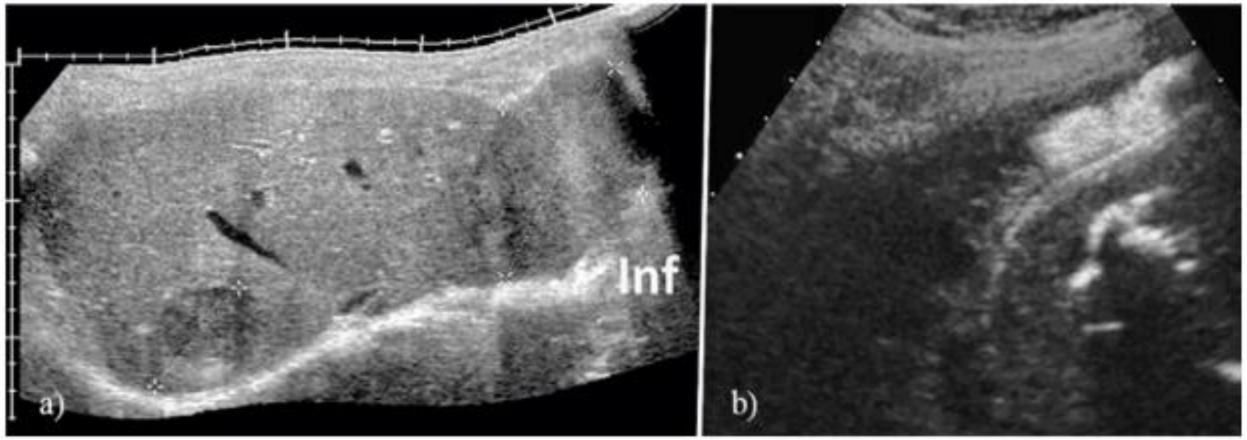

Fig 2. Multiloculated amebiasis (panoramic imaging). The left liver lobe is completely infiltrated (large mass in bet and the surrounding diaphragm and pleura are infiltrated per continuitatem, indicated by "Inf". The right liver lobe al bic abscess (in between markers) (a). A fistula between liver abscess and pleura is shown in (b) using intracavitary coı ultrasound applied during abscess drainage.

Fig 3. Centrally located eosinophilic infiltration in ascariasis (Löffler syndrome). Transient centrally localized infiltrate paracardial in an immunocompromised 16-year-old patient with recurrent intestinal ascariasis and eosinophilia. The US findings are non-specific, but the coarse echoes might represent parasites.

Journal of Ultrasound
https://doi.org/10.1007/s40477-025-01088-7

REVIEW PAPER

POCUS for acute abdominal pain: practical scan protocols on gastrointestinal diseases and an evidence review

Andrea Boccatonda[1] · Alice Brighenti[1] · Valeria Tiraferri[2] · Marisol Doglioli[3,4] · Luca Iazzetta[3,4] · Lucia De Meis[3] · Ehsan Safai Zadeh[5] · Christoph Frank Dietrich[6] · Carla Serra[1]

Received: 4 September 2025 / Accepted: 24 September 2025

Abstract
Acute abdominal pain is a frequent emergency department presentation requiring prompt and accurate diagnosis to guide timely management. Ultrasound imaging plays a critical role in the differential diagnosis of this symptom, offering several advantages including wide availability, cost-effectiveness, and real-time assessment without ionizing radiation. Color and spectral Doppler further enhance diagnostic accuracy by allowing the assessment of blood flow and vascular patterns, which is crucial for identifying ischemic processes. Additionally, ultrasound can help distinguish between gynecological and non-gynecological conditions, such as appendicitis, urinary tract pathologies, or gastrointestinal abnormalities, thereby guiding more targeted investigative pathways or treatment modalities. The rapid, bedside application of ultrasound is especially valuable in unstable patients, ensuring expedited triage and intervention. In certain cases, a negative or inconclusive ultrasound may necessitate further imaging with computed tomography or magnetic resonance imaging. However, ultrasound remains the first-line modality, particularly in pregnant women, to minimize radiation exposure. By integrating ultrasound findings with clinical data and laboratory results, clinicians can establish a precise diagnosis, avoid unnecessary procedures, and initiate timely therapeutic interventions, ultimately improving patient outcomes.

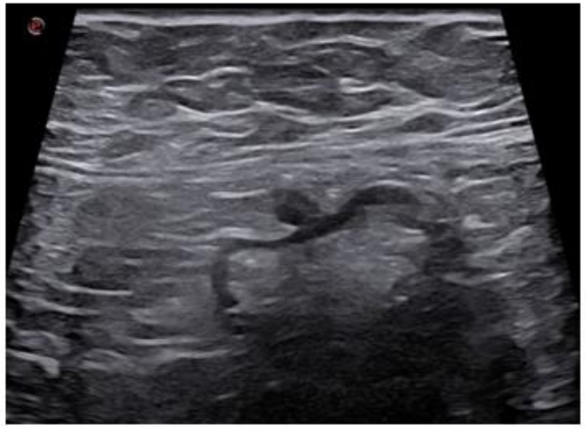

Fig. 3 At the level of the sigmoid colon, several wall diverticula are visible, consistent with diverticulosis. The organ wall shows areas with thickness at the upper limits of normal (2–3 mm). Furthermore, fat stranding is visible around the inflammatory area

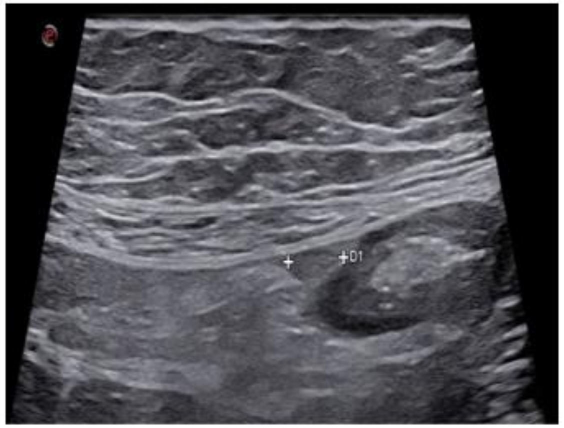

Fig. 4 At the level of the sigmoid colon, several wall diverticula are visible, consistent with diverticulosis. The organ wall shows areas with thickness at the upper limits of normal (2–3 mm). Furthermore, fat stranding is visible around the inflammatory area

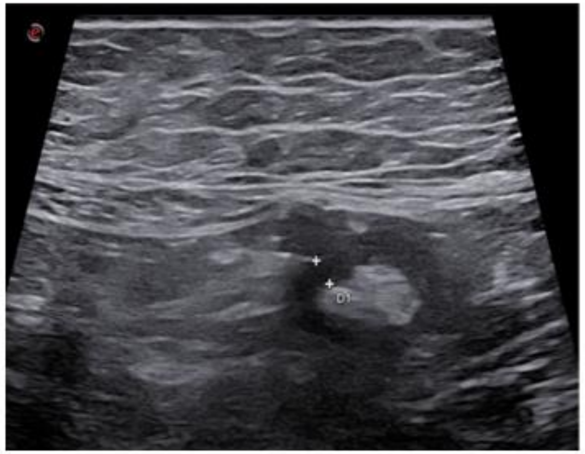

Fig. 5 At the level of the sigmoid colon, several wall diverticula are visible, consistent with diverticulosis. The organ wall shows areas with thickness at the upper limits of normal (2–3 mm). Furthermore, fat stranding is visible around the inflammatory area

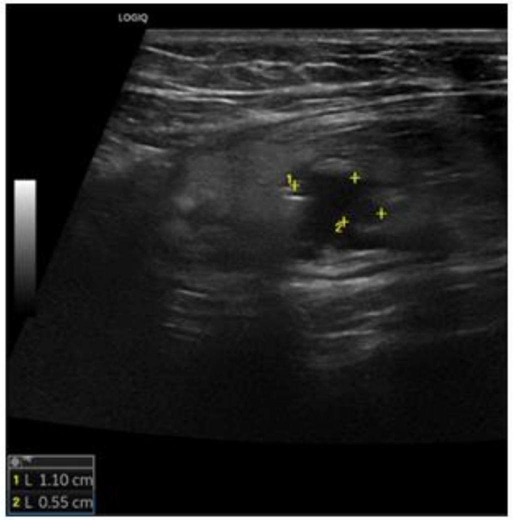

Fig. 6 At the level of the descending colon and sigmoid colon, the wall thickness is at the upper limits (3–4 mm), with preserved wall stratification. A micro-perforated diverticulum is observed, accompanied by a small 11 mm collection and a hyperechoic appearance of the adjacent adipose tissue

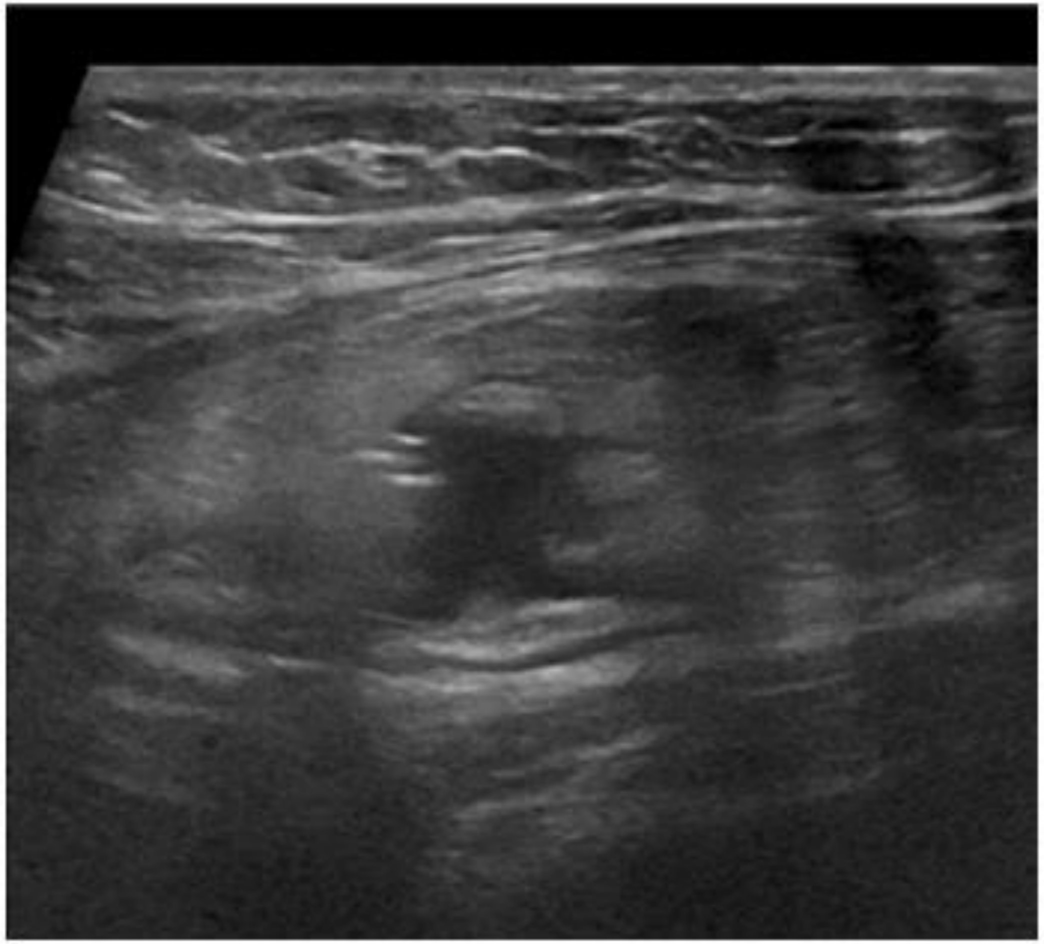

Fig. 7 At the level of the descending colon and sigmoid colon, the wall thickness is at the upper limits (3–4 mm), with preserved wall stratification. A micro-perforated diverticulum is observed, accompanied by a small 11 mm collection and a hyperechoic appearance of the adjacent adipose tissue

Fig. 8 In the right iliac fossa, the final loop of the ileum shows, over a segment of 7 cm, thickened walls measuring 5 mm, with preserved stratification and the presence of vascular signals in the walls as detected by color Doppler imaging (Limberg 3). Another segment, located more proximally in the ileum and observed in the hypogastric region, measures approximately 5 cm, with walls thickened up to 10 mm, loss of stratification, and the presence of vascular signals in the walls on color Doppler imaging (Limberg 4). These segments show a narrowed lumen and dilation of the upstream bowel loop (55 mm diameter)

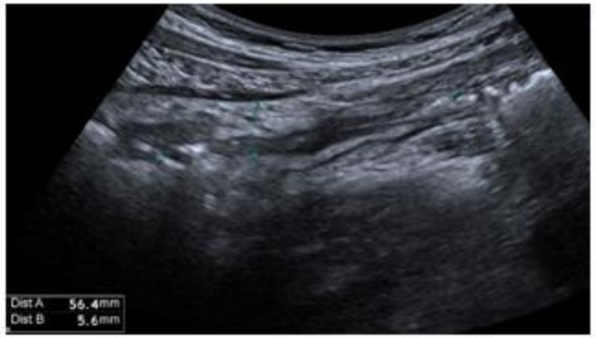

Fig. 9 In the right iliac fossa, the final loop of the ileum shows, over a segment of 7 cm, thickened walls measuring 5 mm, with preserved stratification and the presence of vascular signals in the walls as detected by color Doppler imaging (Limberg 3). Another segment, located more proximally in the ileum and observed in the hypogastric region, measures approximately 5 cm, with walls thickened up to 10 mm, loss of stratification, and the presence of vascular signals in the walls on color Doppler imaging (Limberg 4). These segments show a narrowed lumen and dilation of the upstream bowel loop (55 mm diameter)

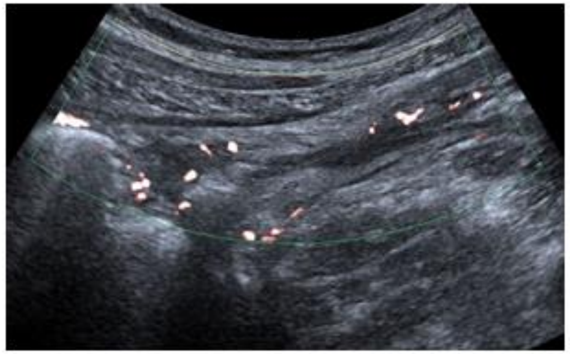

Fig. 10 In the right iliac fossa, the final loop of the ileum shows, over a segment of 7 cm, thickened walls measuring 5 mm, with preserved stratification and the presence of vascular signals in the walls as detected by color Doppler imaging (Limberg 3). Another segment, located more proximally in the ileum and observed in the hypogastric region, measures approximately 5 cm, with walls thickened up to 10 mm, loss of stratification, and the presence of vascular signals in the walls on color Doppler imaging (Limberg 4). These segments show a narrowed lumen and dilation of the upstream bowel loop (55 mm diameter)

Fig. 11 In the right iliac fossa, the final loop of the ileum shows, over a segment of 7 cm, thickened walls measuring 5 mm, with preserved stratification and the presence of vascular signals in the walls as detected by color Doppler imaging (Limberg 3). Another segment, located more proximally in the ileum and observed in the hypogastric region, measures approximately 5 cm, with walls thickened up to 10 mm, loss of stratification, and the presence of vascular signals in the walls on color Doppler imaging (Limberg 4). These segments show a narrowed lumen and dilation of the upstream bowel loop (55 mm diameter)

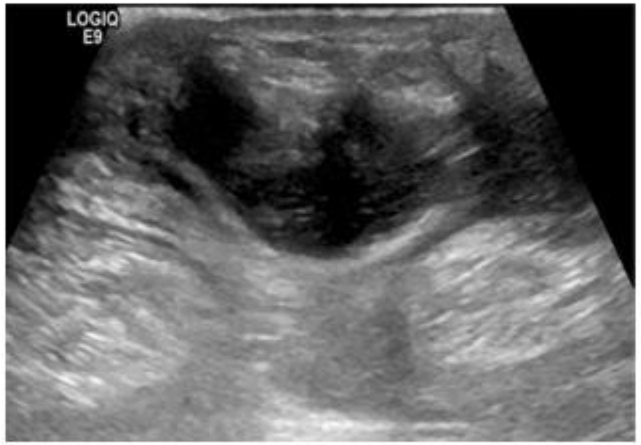

Fig. 12 At the site of the cutaneous fistulous opening, an elongated entero-mesenteric collection with a fistulous tract is visualized. This collection extends anteriorly, just beneath the adipose tissue, and becomes superficial, reaching as close as 7 mm from the skin surface

Fig. 13 At the site of the cutaneous fistulous opening, an elongated entero-mesenteric collection with a fistulous tract is visualized. This collection extends anteriorly, just beneath the adipose tissue, and becomes superficial, reaching as close as 7 mm from the skin surface

Fig. 14 In the left inguinal region, a hernia orifice measuring 10 mm is visible, through which omental fat is protruding, showing weak arterial signals on Doppler imaging. Additionally, a small amount of peri-omental fluid is present

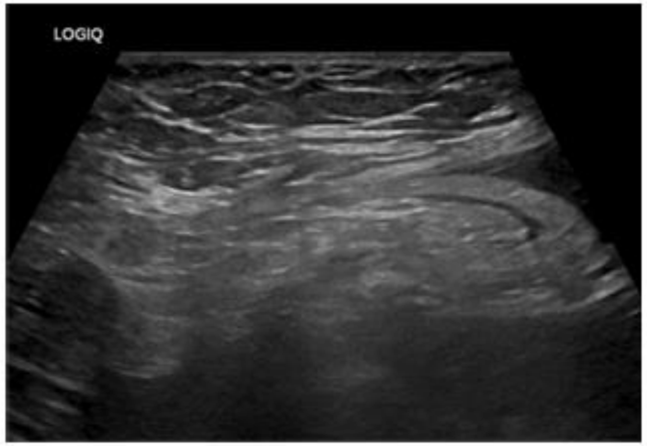

Fig. 15 In the left inguinal region, a hernia orifice measuring 10 mm is visible, through which omental fat is protruding, showing weak arterial signals on Doppler imaging. Additionally, a small amount of peri-omental fluid is present

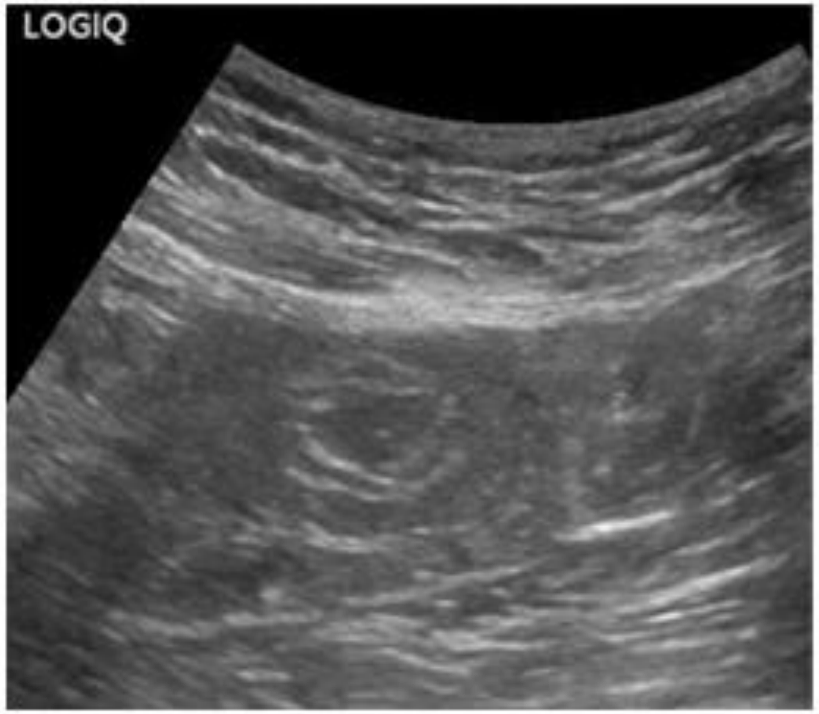

Fig. 16 In the left iliac fossa, in transverse scans, a "target" image is observed, with a typical "loop within loop" configuration visible in longitudinal scans, consistent with intestinal intussusception involving the small intestine

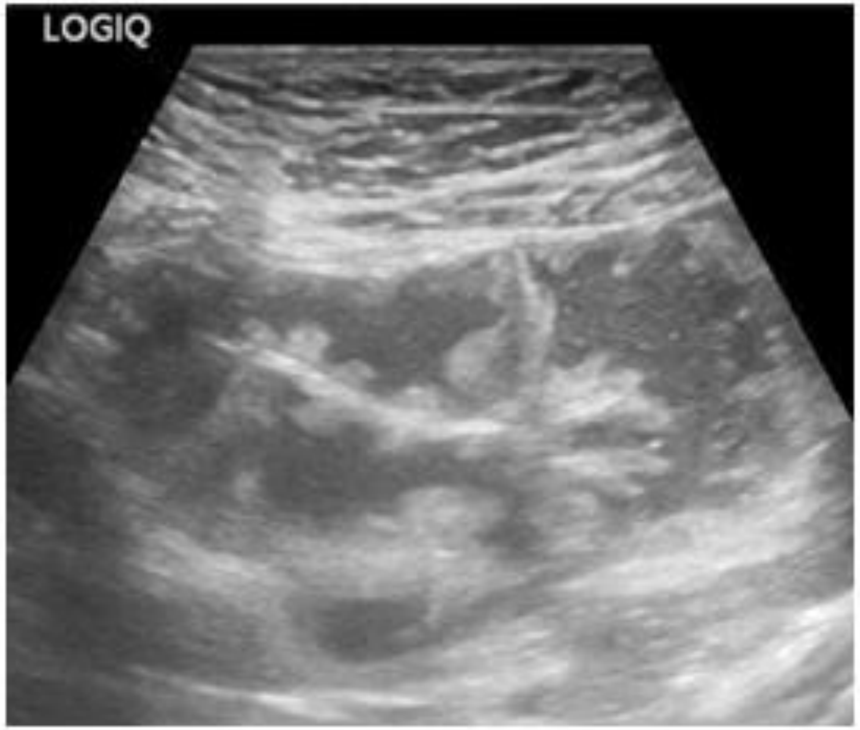

Fig. 18 Proximal to the aforementioned intussuscepted intestinal segment, several distended jejunal loops filled predominantly with fluid material are observed

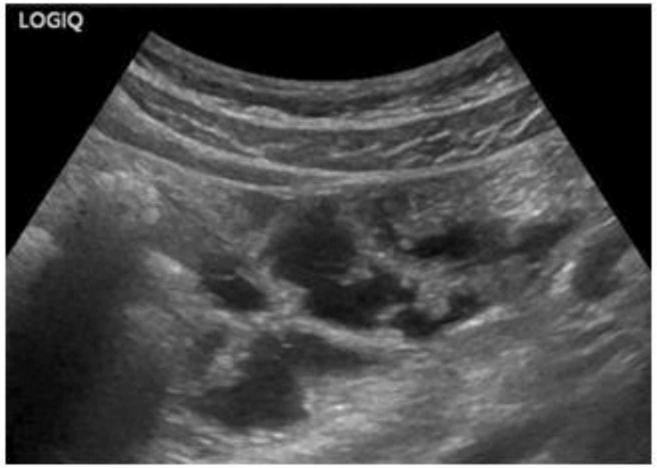

Fig. 19 Proximal to the aforementioned intussuscepted intestinal segment, several distended jejunal loops filled predominantly with fluid material are observed

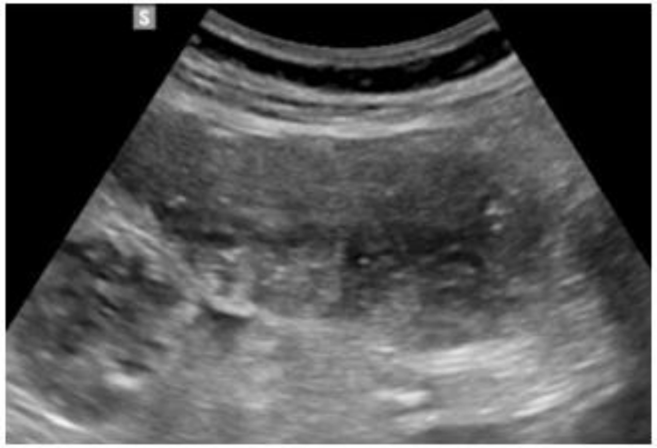

Fig. 20 Jejunal loops appear markedly dilated, with a diameter exceeding 2.5 cm and walls of regular thickness, with the lumen filled predominantly with fluid exhibiting the typical "to-and-fro" movement. Additionally, a slight perivisceral fluid layer is observed

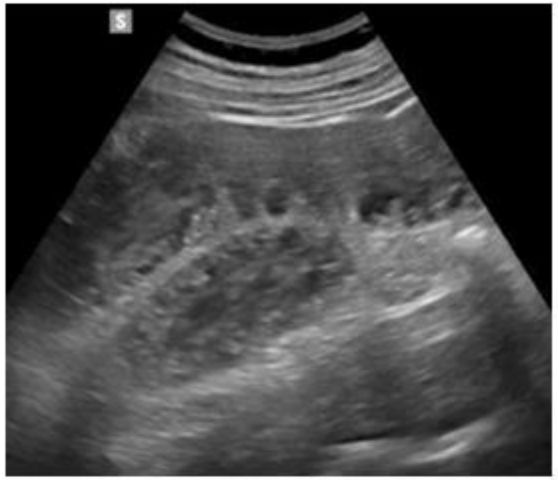

Fig. 21 Jejunal loops appear markedly dilated, with a diameter exceeding 2.5 cm and walls of regular thickness, with the lumen filled predominantly with fluid exhibiting the typical "to-and-fro" movement. Additionally, a slight perivisceral fluid layer is observed

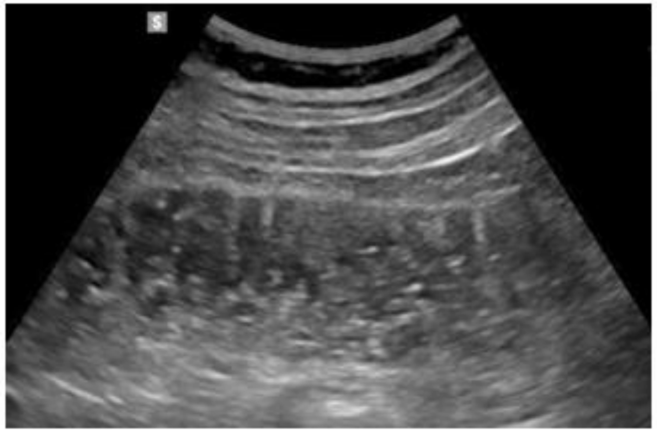

Fig. 22 Jejunal loops appear markedly dilated, with a diameter exceeding 2.5 cm and walls of regular thickness, with the lumen filled predominantly with fluid exhibiting the typical "to-and-fro" movement. Additionally, a slight perivisceral fluid layer is observed

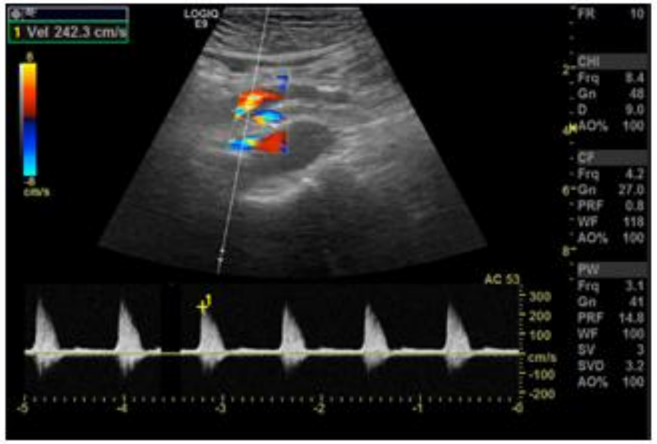

Fig. 27 These images show an ectasia of the mesenteric artery approximately 1.5 cm from its origin, with dimensions of 11 × 10 mm (AP x LL). Within the ectatic segment, an eccentric hypoechoic thrombus is visible along the inferior and lateral walls, with a maximum thickness of 6 mm. The thrombus extends along the course of the artery for approximately 2 cm, causing, at its thickest point, a stenosis of about 50–60%

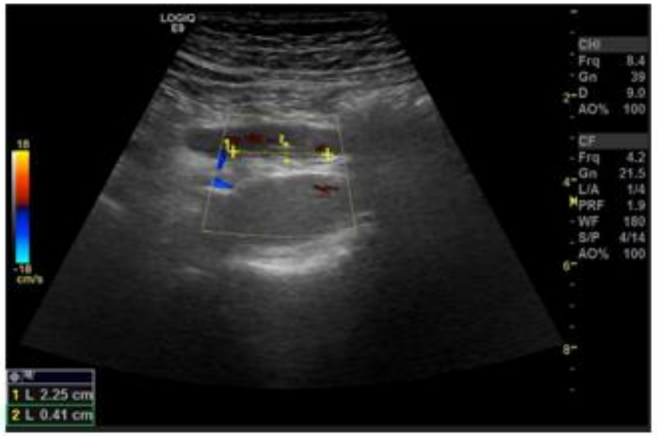

Fig. 28 These images show an ectasia of the mesenteric artery approximately 1.5 cm from its origin, with dimensions of 11 × 10 mm (AP x LL). Within the ectatic segment, an eccentric hypoechoic thrombus is visible along the inferior and lateral walls, with a maximum thickness of 6 mm. The thrombus extends along the course of the artery for approximately 2 cm, causing, at its thickest point, a stenosis of about 50–60%

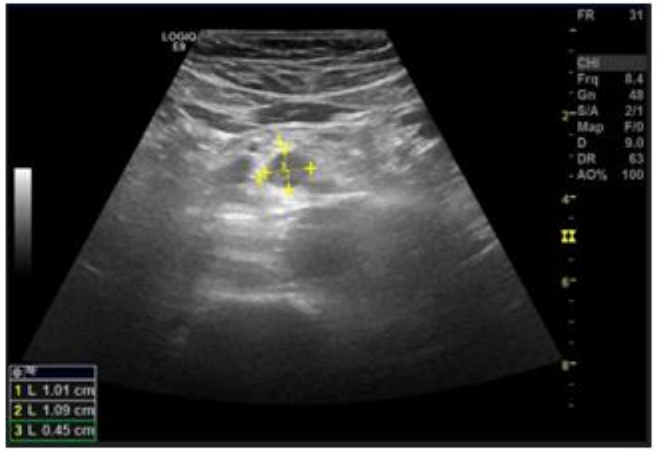

Fig. 29 These images show an ectasia of the mesenteric artery approximately 1.5 cm from its origin, with dimensions of 11 × 10 mm (AP x LL). Within the ectatic segment, an eccentric hypoechoic thrombus is visible along the inferior and lateral walls, with a maximum thickness of 6 mm. The thrombus extends along the course of the artery for approximately 2 cm, causing, at its thickest point, a stenosis of about 50–60%

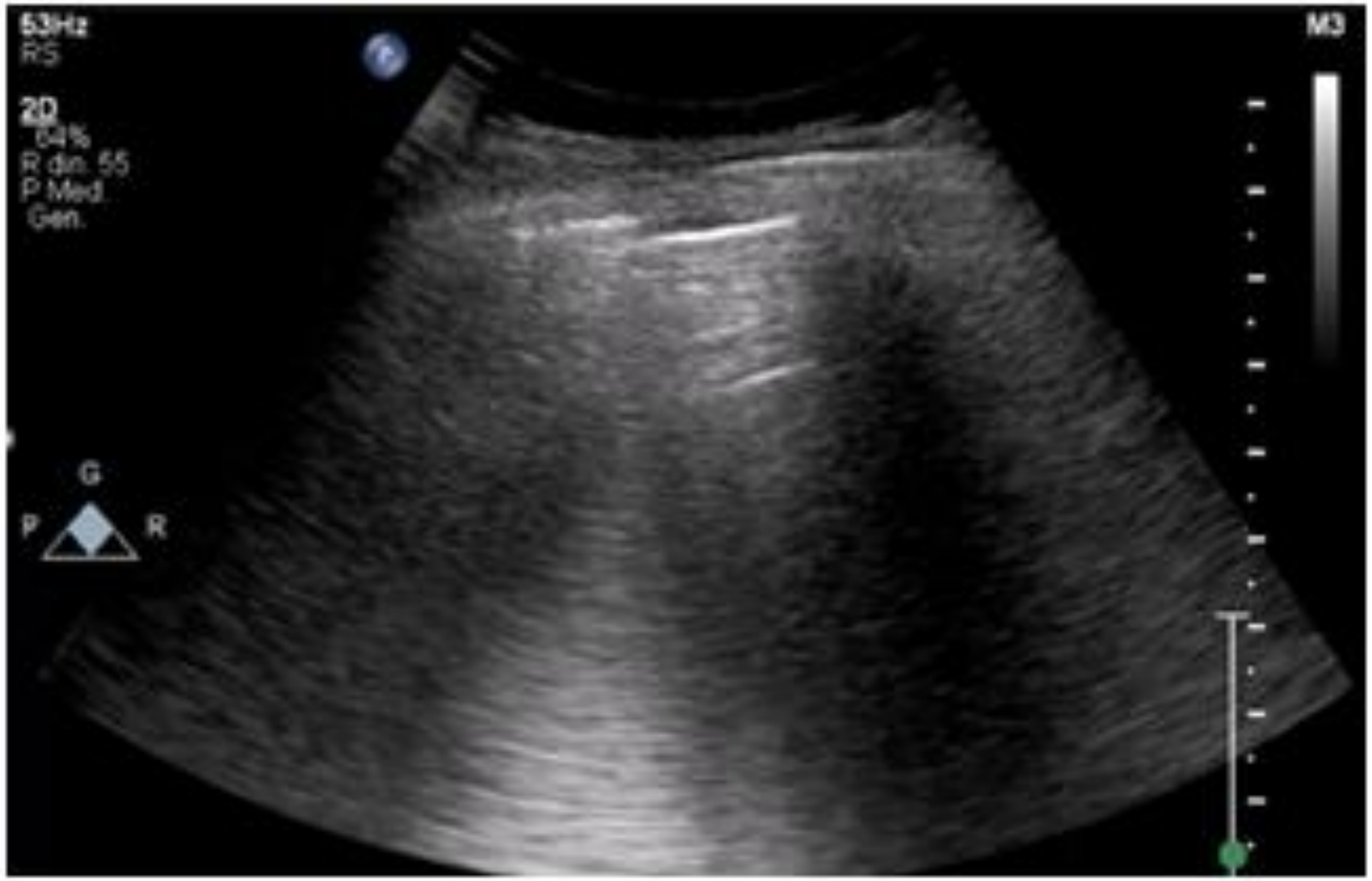

Fig. 30 Image of pneumoperitoneum: air artifacts (similar to lung artifacts) are seen beneath the diaphragm in an intraperitoneal location. The patient is examined in the left lateral decubitus position with a right coronal scan. The air artifacts obscure visualization of the liver

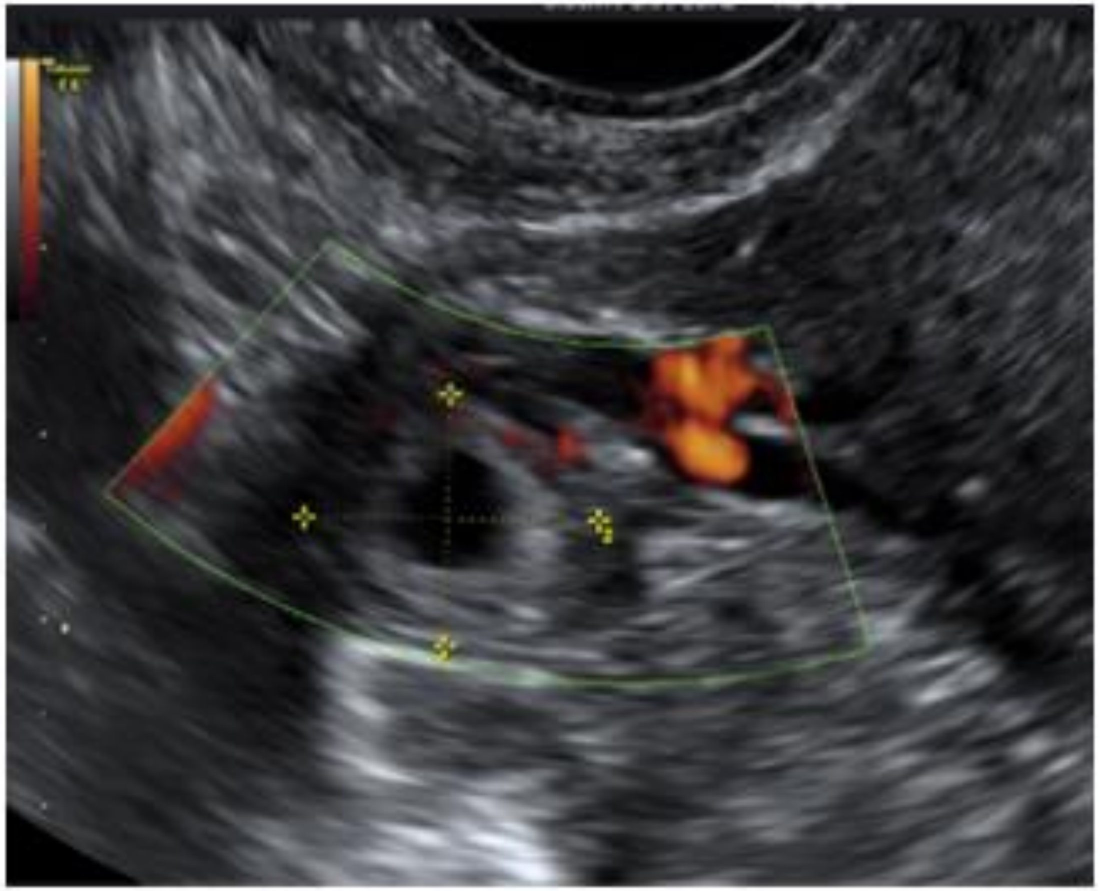

Fig. 31 Transverse color Doppler scan showing a hyperechoic tubal ring of an ectopic gestation with no blood flow in the echogenic ring surrounding the gestational sac

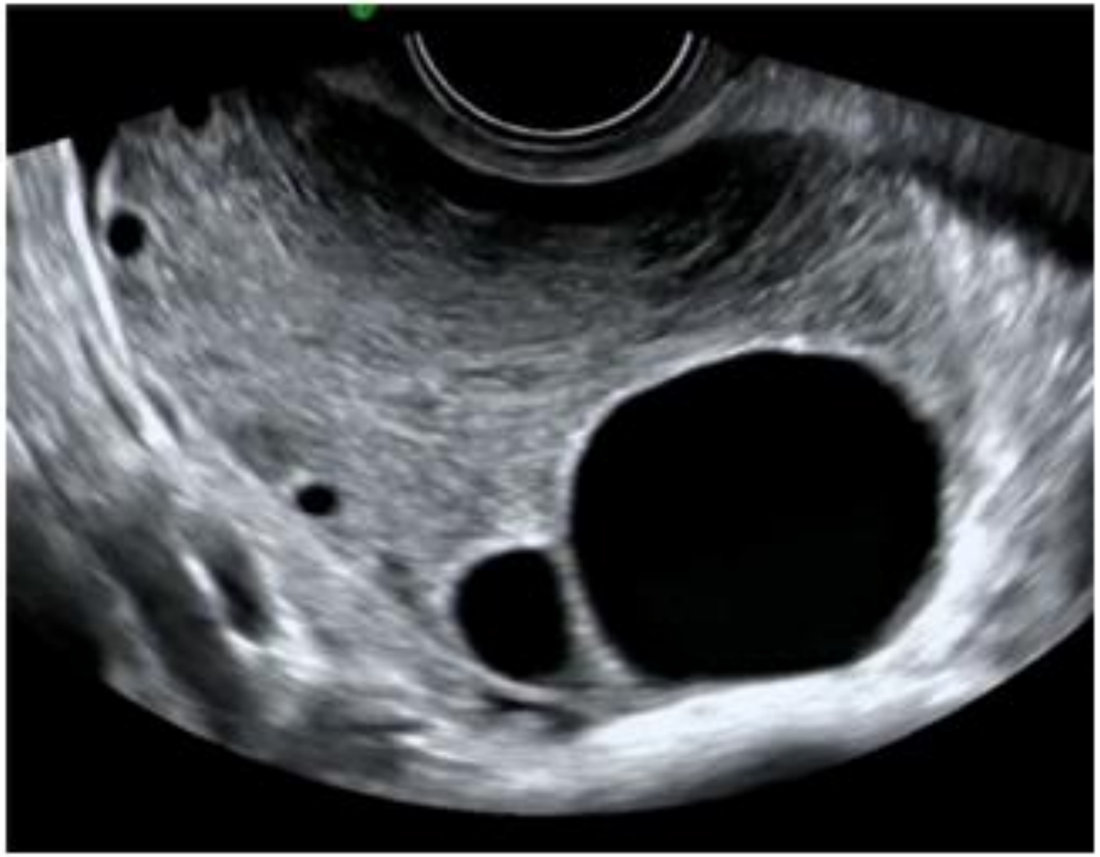

Fig. 32 Ovarian torsion showing an enlarged and edematous with heterogeneous echotexture parenchyma with peripherally located follicles ("string of pearls" sign) and perifollicular hyperechoic rim ("follicular ring sign")

ORIGINAL ARTICLE

Comparison of Lung Ultrasound Findings in Patients with Pulmonary Tuberculosis and Lobar Pneumonia: A Case–control Study

Devaraj, Uma*; Veluthat, Chitra; Venkatnarayan, Kavitha; Krishnaswamy, Uma Maheswari; Ramachandran, Priya

Author Information

Journal of Medical Ultrasound 33(3):p 216-221, Jul–Sep 2025. | ***DOI:*** 10.4103/jmu.jmu_52_24

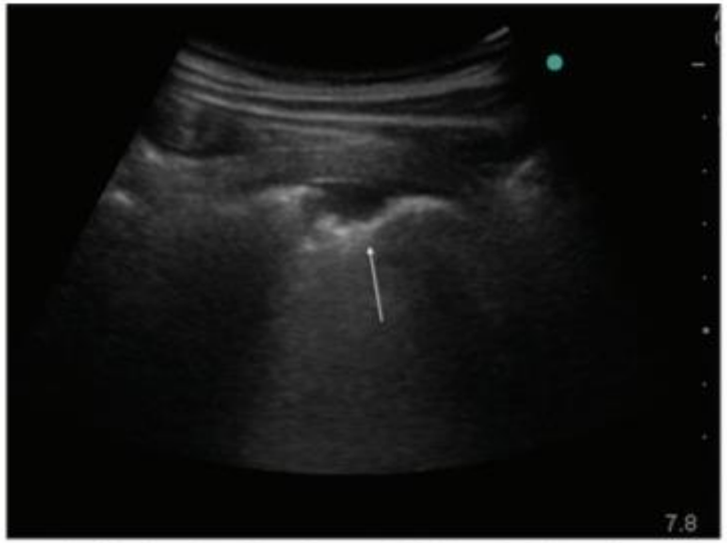

Figure 3: Sub pleural nodules. Arrows: Subpleural nodules, characterized by parenchymal subpleural hypoechoic region with posterior acoustic enhancement

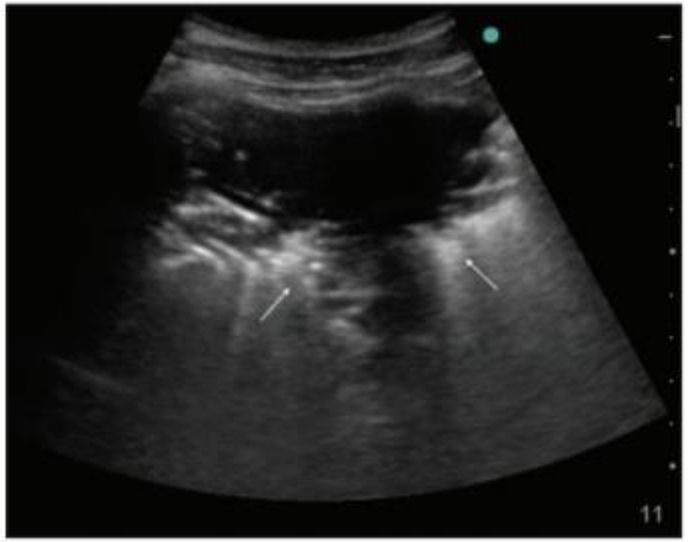

Figure 5: Shred sign. Arrow points to shred sign characterized by hyperechoic, broken, and irregular line at the deep edge of the sonological image, in the consolidated area of the lung

good with a kappa coefficient value of 0.85. The time taken to complete LUS ranged from 3 to 6 min.

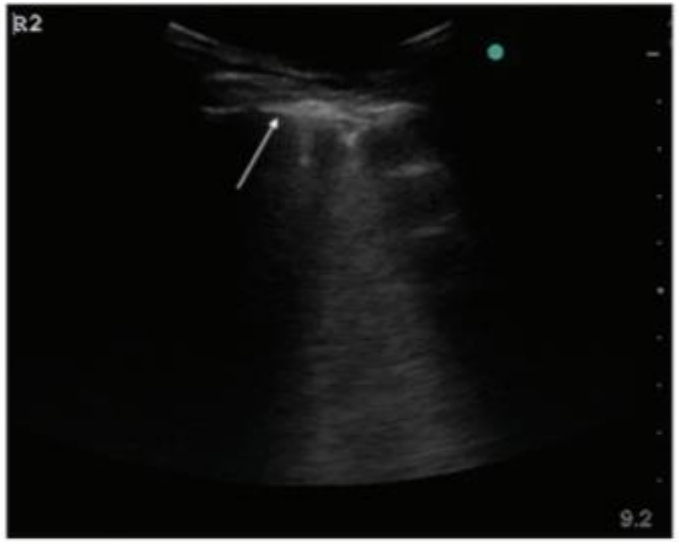

Figure 4: Irregular pleura. Arrow: Irregular pleura

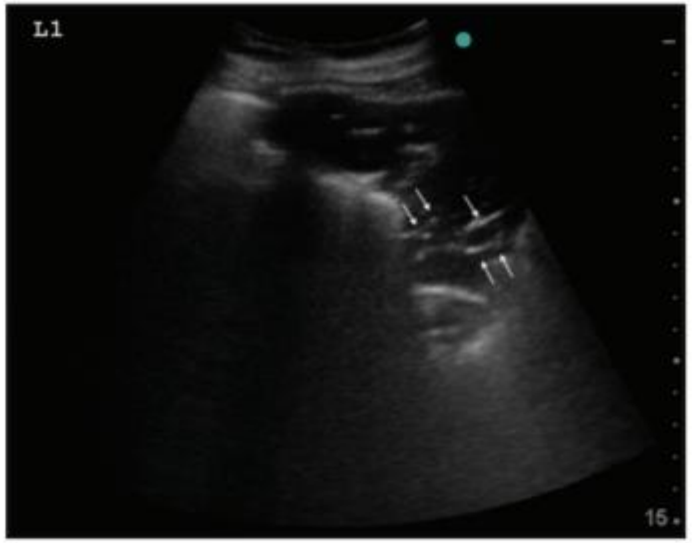

Figure 6: Air-bronchogram characterized by hyperechoic branching image within the hypoechoic area with shredded margins. Arrows show the air-bronchogram

Original Article

Comparison of Lung Ultrasound Findings in Patients with Pulmonary Tuberculosis and Lobar Pneumonia: A Case–control Study

Uma Devaraj*, Chitra Veluthat, Kavitha Venkatnarayan, Uma Maheswari Krishnaswamy, Priya Ramachandran

Department of Pulmonary and Sleep Medicine, St. John's Medical College, Bengaluru, Karnataka, India

Abstract

Background: The utility of lung ultrasound (LUS) in diagnosing respiratory disorders is being studied only in recent times. We aimed to describe the ultrasound (USG) features of pulmonary tuberculosis (TB) and compare them with those of lobar pneumonia. In addition, the LUS findings of both diseases were corroborated with chest X-ray findings. **Methods:** The study subjects consisted of adult subjects recently diagnosed with pulmonary TB and those diagnosed with lobar pneumonia. Both subsets of patients underwent LUS evaluation. **Results:** Ninety-six subjects with 64 microbiologically confirmed TB and 32 lobar pneumonia patients were included. The study subjects' mean age was 46.78 ± 15.75 years and the majority were males (n = 62; 64.6%). LUS showed focal interstitial pattern, cavity, and irregular pleura in TB patients which were significantly different ($P \leq 0.001$) from the findings of air bronchogram and/or shred sign seen in patients with lobar pneumonia. The overall sensitivity of LUS compared to X-ray, to identify abnormalities in TB and lobar pneumonia patients, was 88.6%. The LUS and CXR findings were concordant in 93.75% of TB patients and 90.6%) of lobar pneumonia patients. Additional USG abnormalities other than that seen on CXR were demonstrated in 13 (20.3%) TB patients. **Conclusion:** LUS is a valuable tool to detect TB and lobar pneumonia and can discriminate between the two conditions. LUS performance was on par with CXR in the detection of abnormalities. The lack of radiation exposure and portability of LUS makes it an attractive tool for bedside use as well as in field conditions where radiography may not be readily available.

Keywords: Focal interstitial pattern, lobar pneumonia, lung ultrasound, pulmonary tuberculosis

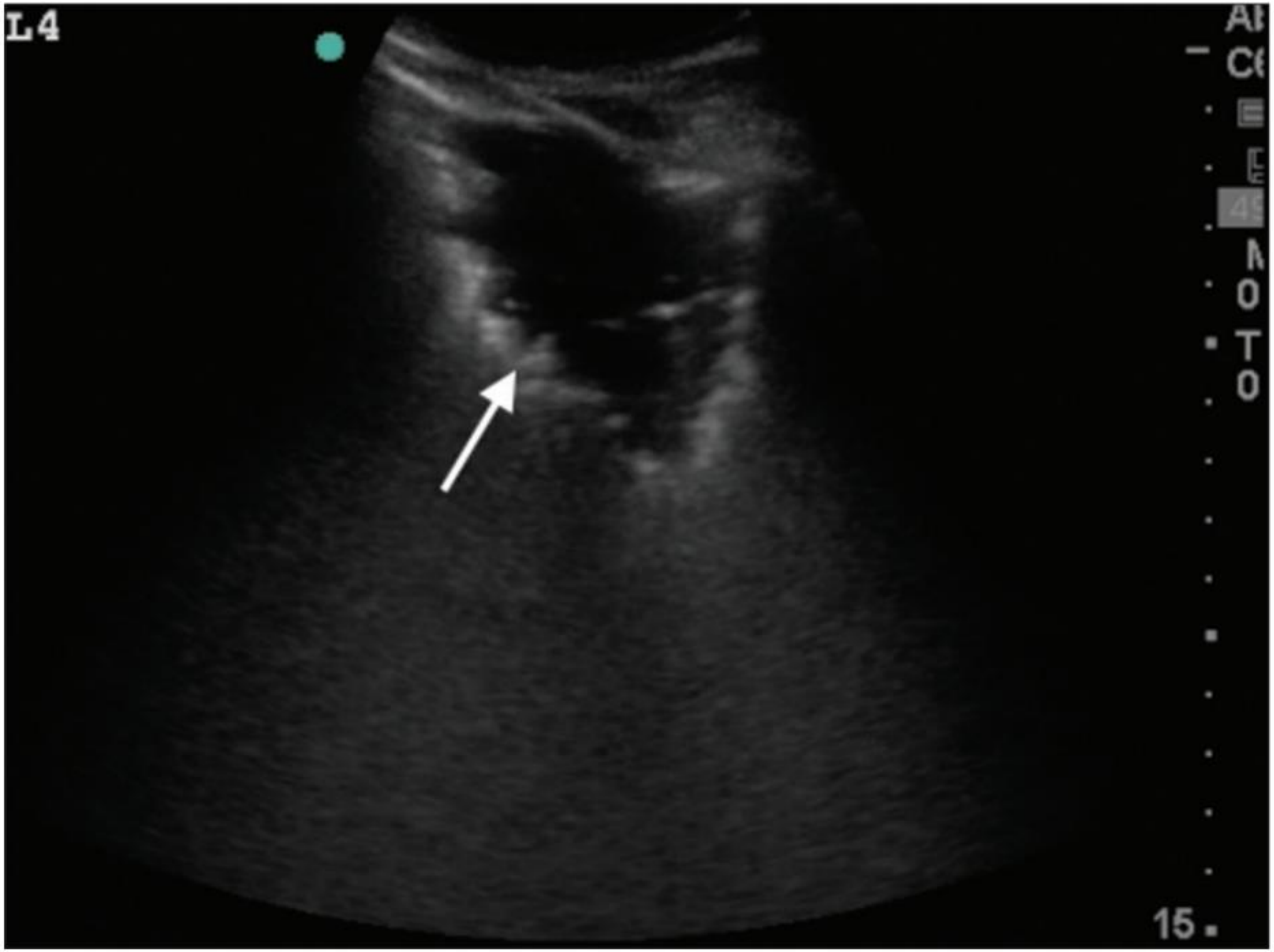

Figure 7: Cavity characterized by hypoechoic area with surrounding shred sign. Arrow points to the shred sign

Ahead of print

Med Ultrason 2025:0, 1-3 Online first
DOI: 10.11152/mu-4532

Incidental finding of gallbladder aspergilloma; a rare occurrence

Nils Raab[1], Bernd Stephan[1], Sabin Khatri[1], Michael Wöhlke[2], Raoul Hinze[2], Christoph Frank Dietrich[3]

[1]LUP-Kliniken Helene von Bülow KH Ludwigslust, Gastroenterologie, Ludwigslust, Germany, [2]Helioskliniken Schwerin, Institut für Pathologie, Schwerin, Germany, [3]Department Allgemeine Innere Medizin (DAIM), Kliniken Hirslanden Beau Site, Salem und Permanence, Bern, Switzerland

Abstract

The value of an ultrasound prior to planned interventions is undisputed. Clinically relevant incidental findings are also among the reasons why abdominal ultrasound examinations should be considered part of the diagnostic evaluation during inpatient admission. We report here an interesting case of an unusual “three-headed” polypoid lesion on ultrasound, which histologically and pathologically revealed a saprophytic manifestation of local aspergillosis in the gallbladder without clinical signs of cholecystitis.

Keywords: cholecystitis; parasitosis; inflammation; gallbladder carcinoma; gallbladder polyps

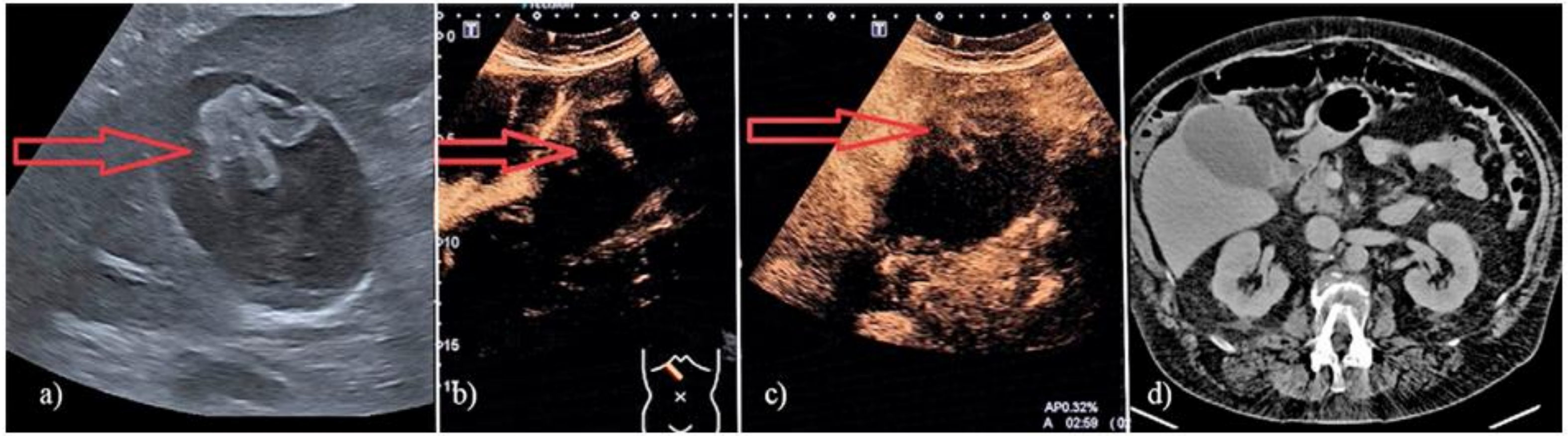

Fig 1. Conventional B-scan ultrasound with 3.5 cm polyp structure in the gallbladder (a) and CEUS in the arterial (b) phase and late phase (c); d) Computed tomography (axial and coronal section) [Dr. H. Kautz Ludwigslust]. The bizarre mass seen on ultrasound within the gallbladder cannot be clearly defined; only a slight inhomogeneous thickening of the wall. The finding is not "shadowing" and therefore escapes detection in computed tomography. An MRI was not possible because of a pacemaker.

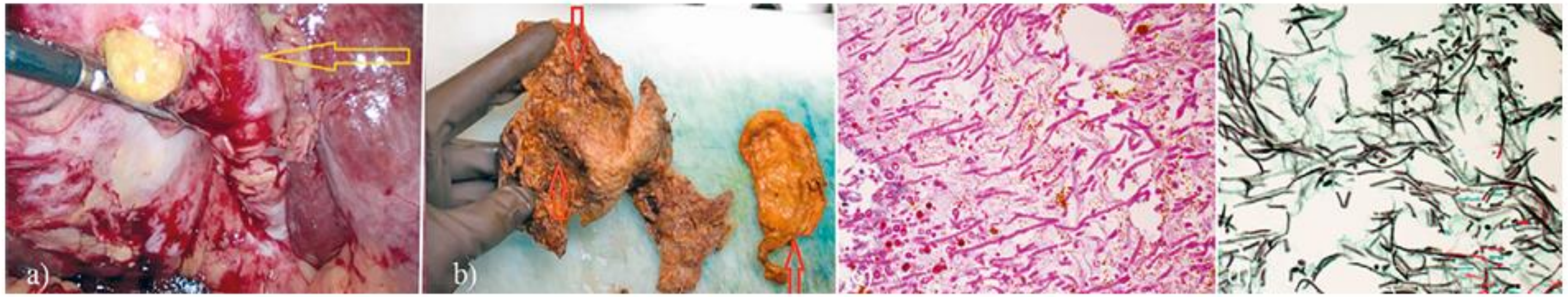

Fig 2. a) Intraoperative site. Inflammatory wall changes are visible. The organ borders and the D. cysticus cannot be clearly delineated; b) Pathology, macroscopic findings (gallbladder, 9.5 cm long): The gallbladder wall is firm to palpation and moderately thickened. The mucosa is focally gloomy with yellowish roughened areas. No evidence of concrements. A piece of soft tissue measuring 7.0x3.7x0.3 cm with a lumen is enclosed with the specimens. A tissue stalk up to 3.8 cm long is attached to this corresponding to the sonographically detectable GB polyp. These were masses of fungal structures (molds) (Helios Clinics Schwerin, OA Dr. Wölke, CA Dr. R. Hinze); c) Microscopic findings (gallbladder): Extensive mucosal ulceration with focal deep wall necrosis affecting the entire GB. Superficial concremental residues with partly giant cell foreign body reaction. Granulation tissue is histologically developed in all GB sections. Thickness varies between 1.5 and 8 mm. PAS400 stain and d) fungal structures [Crocott400 stain] [Pathology Dr. M. Wöhlke].

Research paper

Cite as: Batis V, Detorakis E, Schiza S, Prokopakis E, Krasagakis K, Drakonaki E: Ultrasound imaging in floppy eyelid syndrome: anatomical and clinical considerations. J Ultrason 2025; 25: 19. doi: 10.15557/JoU.2025.0019.

Submitted: 16.03.2025
Accepted: 10.06.2025
Published: 30.06.2025

Ultrasound imaging in floppy eyelid syndrome: anatomical and clinical considerations

Vasilios Batis[1], Efstathios Detorakis[1], Sophia Schiza[2], Emmanuel Prokopakis[3], Konstantinos Krasagakis[4], Elena Drakonaki[5]

[1] *Department of Ophthalmology, School of Medicine, University of Crete, Greece*
[2] *Department of Respiratory Medicine and Sleep Disorders Unit, School of Medicine, University of Crete, Greece*
[3] *Department of Otorhinolaryngology and Laboratory of Translational Otorhinolaryngology Research, School of Medicine, University of Crete, Greece*
[4] *Department of Dermatology, Medical School, University of Crete, Greece*
[5] *Department of Anatomy, School of Medicine, University of Crete, Greece*

Corresponding author: Elena Drakonaki; e-mail: drakonaki@yahoo.gr

DOI: 10.15557/JoU.2025.0019

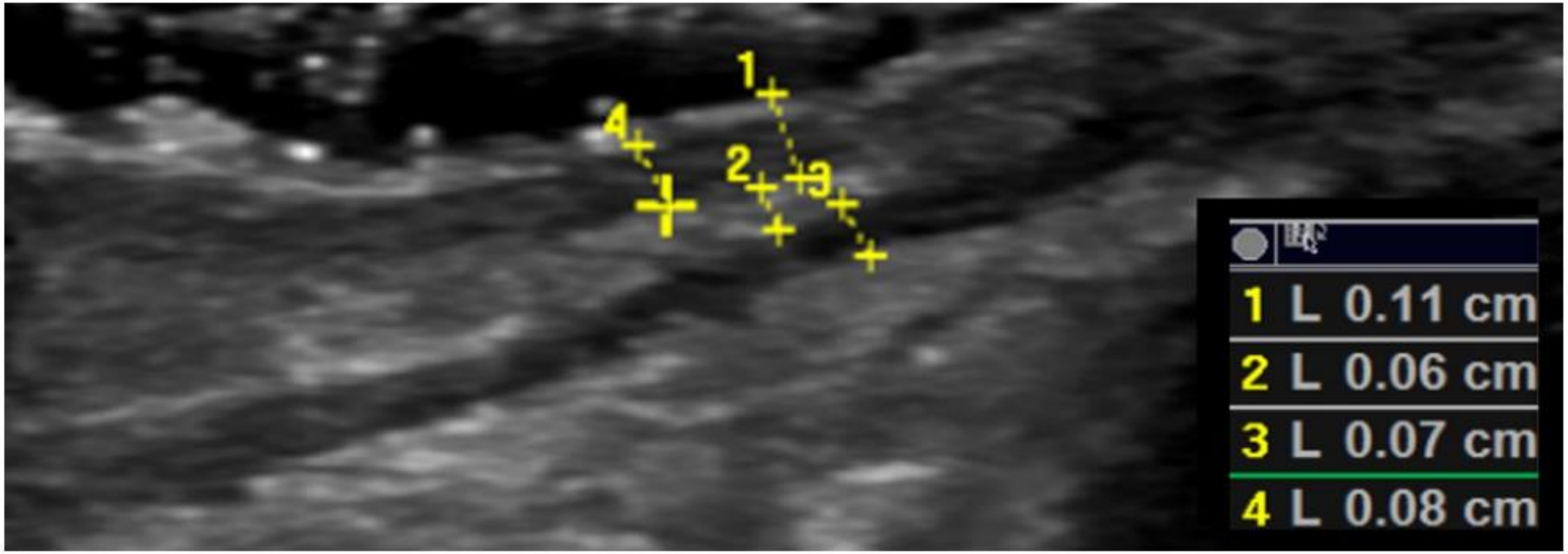

Fig. 1. *Segmentation of upper eyelid anatomical layers in high-frequency ultrasound imaging of the skin (HFUS). HFUS image of the upper eyelid using a high-frequency (8–18 MHz) linear array hockey stick transducer and the standard "MSK superficial" setting of the manufacturer, showing the anatomical layers of the eyelid soft tissue. The thickness of each layer is measured using the system's built-in software tool (calipers) as follows: Measurement 1: Thickness of the most superficial epidermis-dermis layer thickness (EDT), extending from the skin surface to the subcutaneous layer, including the subepidermal low echogenicity band (SLEB). Measurement 2: Thickness of the hyperechoic subcutaneous layer, extending from the deep SLEB to the surface of the underlying muscle (SFT). Measurement 3: Thickness of the palpebral part of the orbicularis oculi muscle, demonstrated as hypoechoic linear muscle fibers (OOT). Measurement 4: Thickness of the SLEB, presenting as a thin band of lower echogenicity at the deepest part of the epidermis-dermis layer*

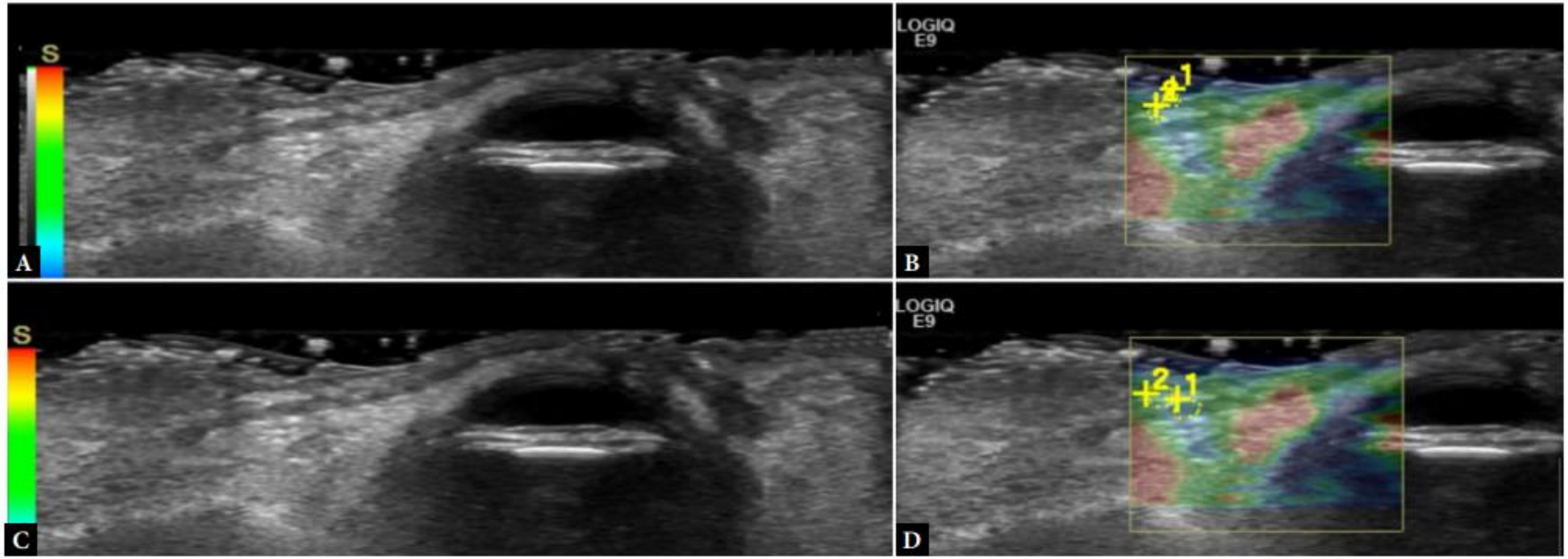

Fig. 2. *Strain elastography (SE) of the upper eyelid.* **A**, **B.** *Epidermis and dermis layer. B-mode image (***A***) and corresponding elastography image (***B***), with color code showing the elasticity scale. The elasticity ratio of the upper eyelid epidermis and dermis layer relative to the subcutaneous fat (skin-to-subcutaneous fat ratio, SFR, A/B) is measured using manually applied ROIs located in the skin (1) and in the fat (2). The respective elasticity values and ratio are automatically calculated and displayed on the screen.* **C**, **D.** *Orbicularis oculi muscle layer. B-mode image (***C***) and corresponding elastography image (***D***), with color code showing the elasticity scale. The elasticity ratio of the orbicularis oculi muscle layer to subcutaneous fat (orbicularis-to-fat ratio, OFR, A/B) is measured using manually applied ROIs located in the muscle (1) and in the fat (2). The respective elasticity values and ratio are automatically calculated and displayed on the screen*

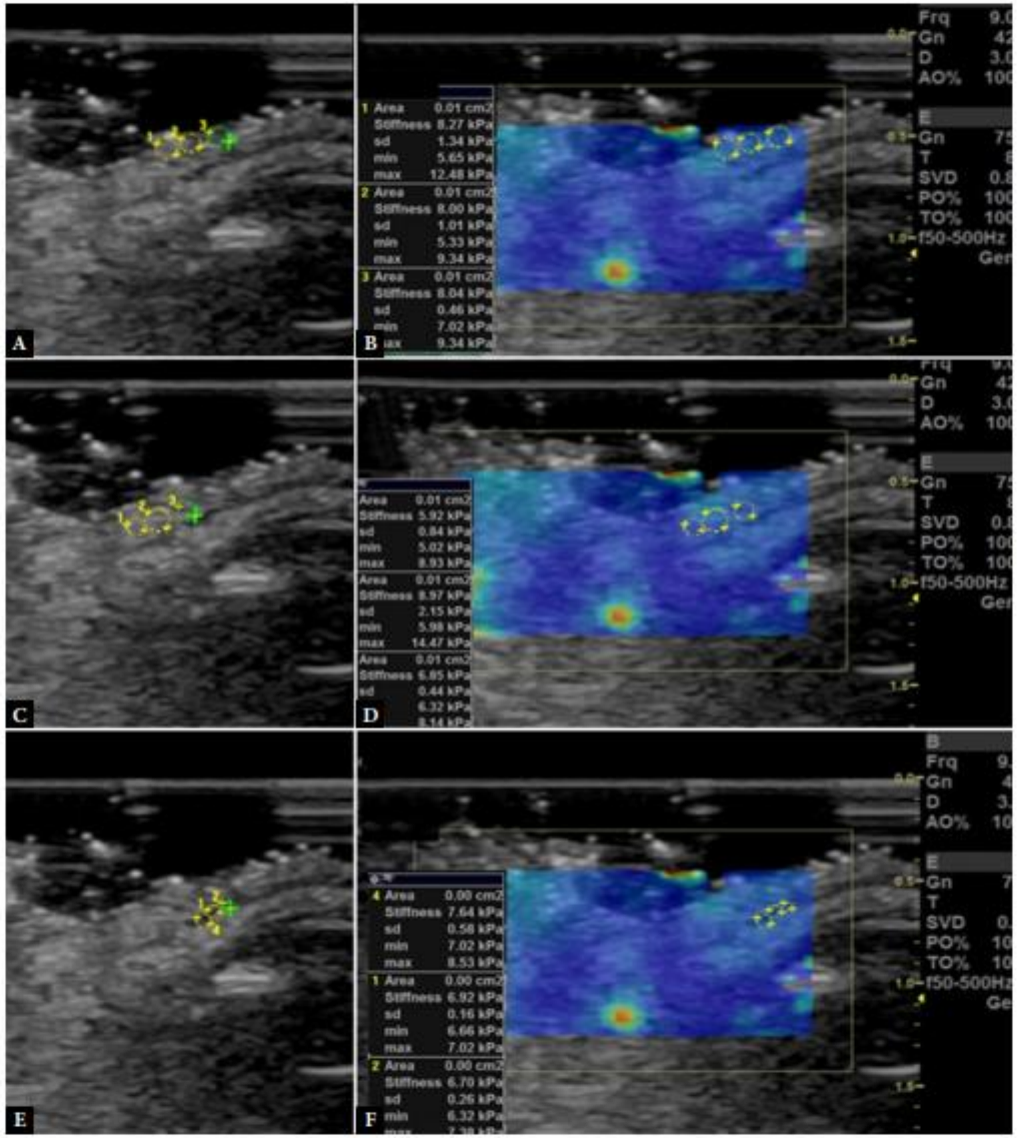

Fig. 3. *Shear wave elastography (SWE) of the upper eyelid.* **A**, **B**. *Superficial epidermis-dermis layer. B-mode image (***A***) and superimposed SWE color coded image showing the elasticity scale (***B***). Three SWE measurements are performed using circular ROIs manually placed on the imaged area. The quantitative assessment of elasticity in kPa (mean value, maximum, minimum, standard deviation) is presented in a superimposed table.* **C**, **D**. *Subcutaneous fat layer. B-mode image (***C***) and superimposed SWE color-coded image showing the elasticity scale (***D***). Three SWE measurements are performed using circular ROIs manually placed on the subcutaneous fat layer. The quantitative assessment of elasticity in kPa (mean value, maximum, minimum, standard deviation) is presented in a superimposed table.* **E**, **F**. *Orbicularis oculi muscle layer. B-mode image (***E***) and superimposed SWE color-coded image showing the elasticity scale (***F***). Three SWE measurements are performed using circular ROIs manually placed on the orbicularis oculi muscle. The quantitative assessment of elasticity in kPa (mean value, maximum, minimum, standard deviation) is presented in a superimposed table. In all cases, only the mean value was used for statistical analysis*

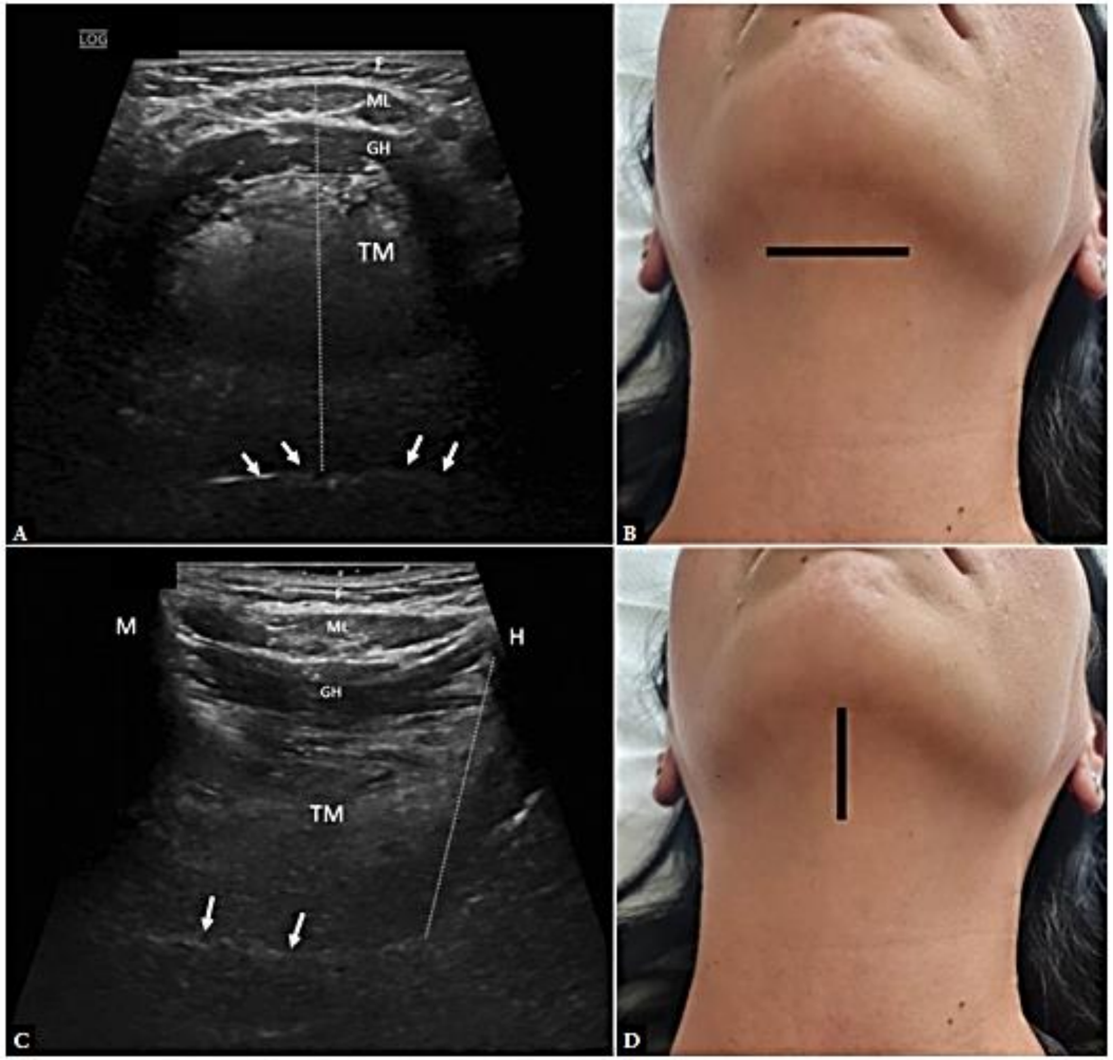

Fig. 4. A. *Tongue thickness (TT) measurement as the anteroposterior diameter between the echogenic mucosa (arrow) and the surface of the mylohyoid muscle (ML) at the floor of the mouth (dotted line).* **B.** *Corresponding placement of the ultrasound probe over the neck area. GH – geniohyoid; TM – intrinsic and extrinsic (genioglossus) muscles of the tongue, ML – mylohyoid muscle; F – subcutaneous fat.* **C.** *Upper airway length (UAL) measurement as the antero-posterior diameter between the anterior edge of the hyoid bone (H) and the hyperechoic line corresponding to the air column at the edge of the hard palate (arrows) (***D***) respective placement of the ultrasound probe over the neck area. GH – geniohyoid; TM – intrinsic and extrinsic (genioglossus) muscles of the tongue; ML – mylohyoid muscle; F – subcutaneous fat; H – hyoid bone shadow; M – mandible shadow*

Tab. 2. Upper eyelid and submental tissue USE, SE, and SWEI parameter measurements (mean ± SD, range), with associated levels of statistical significance

Ahead of print

Med Ultrason 2025:0, 1-12 Online first
DOI: 10.11152/mu-4500

Why and when are activity scores and advanced ultrasound techniques needed in inflammatory bowel disease (IBD)?

Christian Jenssen[1], Frauke Petersen[2], Michael Höpfner[3], Dieter Nürnberg[4], Deike Strobel[5], Johanna Vogelpohl[6], Christoph F Dietrich[7]

Abstract

In addition to avoidance of radiation exposure, the main advantages of ultrasound diagnostics in inflammatory bowel disease (IBD) patients are its' immediate availability, also as a component of the physical examination (extended point of care), its' repeatability and its' high patient comfort. The fact that the examination is carried out directly by the treating physician and is not delegated to the radiologist increases compliance and therapy adherence of the patients.

In the current series of papers a synopsis of recommendations for ultrasound in IBD guidelines, ultrasound parameters in inflammatory bowel disease including activities scores, the value of contrast enhanced ultrasound (CEUS), small intestinal contrast ultrasound (SICUS) and elastography, perineal ultrasound (PNUS), endoscopic ultrasound (EUS) including endorectal ultrasound (ERUS), interventional ultrasound (INVUS), detection of disease complications (stenoses, fistula, abscess), extraintestinal manifestations, differential diagnosis, evaluation of treatment response and outlook are discussed and illustrated.

Keywords: gastrointestinal tract; ultrasound; magnetic resonance imaging; computed tomography; endosonography

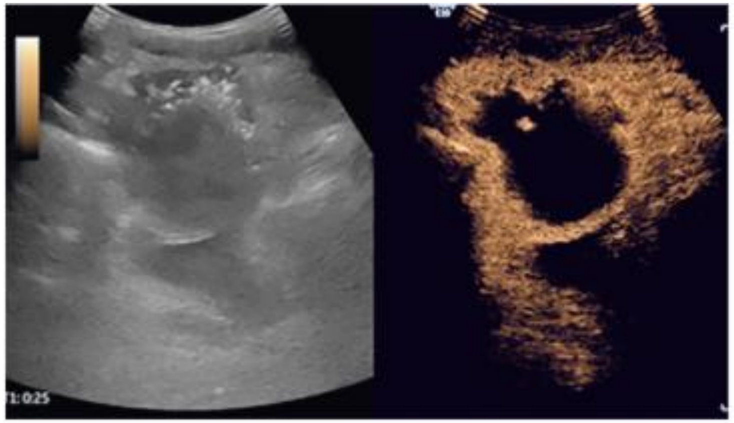

Fig 1. CEUS in intestinal ultrasound, abscess: 1-3 MHz probe, MI 0.08, 1.4 ml Sonovue®, lower abdomen, medial sagittal plane. Image on the left without contrast showing a mass bulging into the bladder, with gas reflexes at the ventral aspect, but apparently solid underneath. Contrast injection shows the mass completely avital, with a hyperenhancing rim typical for an abscess.

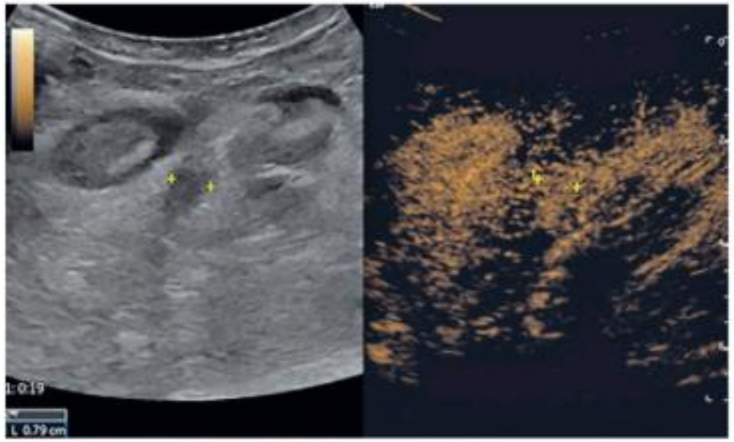

Fig 2. CEUS in intestinal ultrasound: ruling out abscess. 1-3 MHz curved array probe, MI 0.08, 1.4 ml Sonovue®. Inflammatory bowel loop in Crohn's disease, small hypoechoic zone in between the inflamed ileum parts. Contrast ultrasound at the left part of the image shows rich perfusion in this zone ruling out an abscess. Beginning fistula suspected.

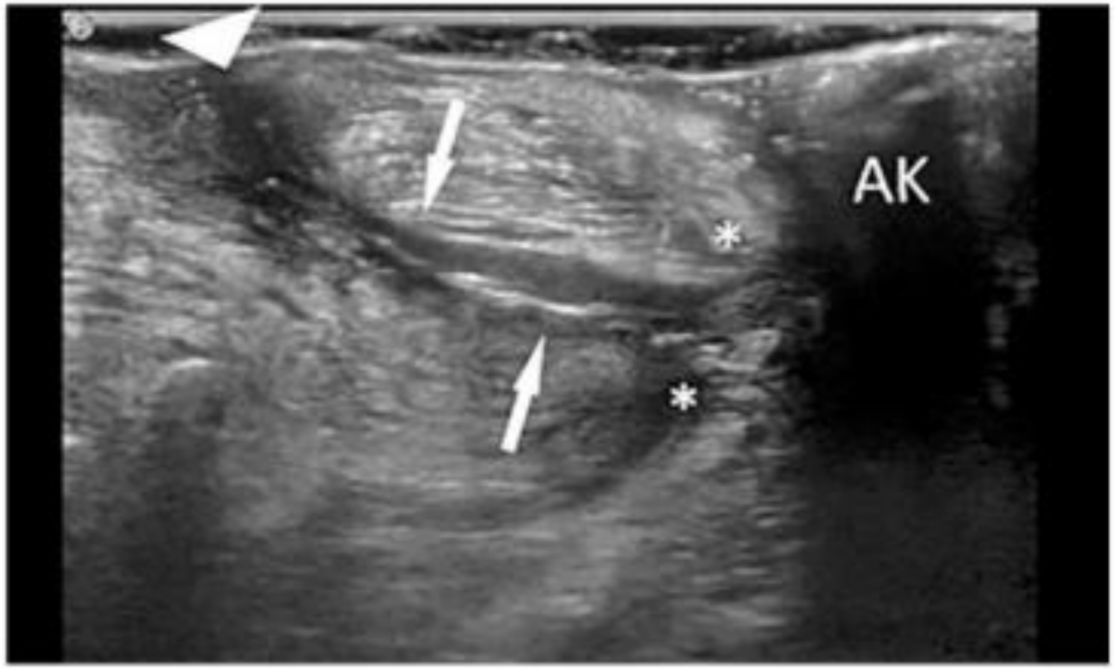

Fig 3. Visualisation of a transsphincteric fistula by PNUS in a patient with Crohn's disease: the fistula presents with hypoechoic wall surrounding the central echogenic luminal reflex (arrows) and reaches the anal lumen (AK: anal channel) traversing the hypoechoic structure of the internal anal sphincter (*). The perianal fistula opening (arrowhead) is clearly visible, surrounded by hypoechoic phlegmonous inflammation.

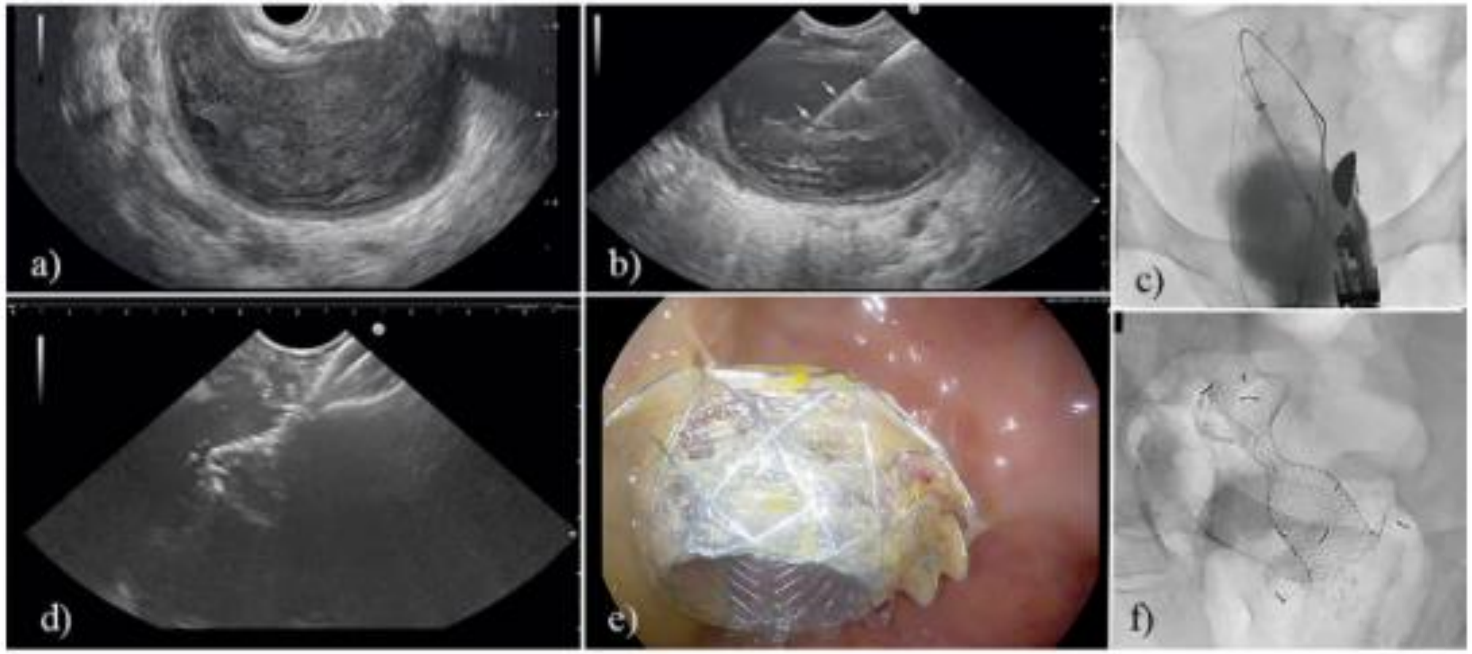

Fig 7. Endoscopic ultrasound (EUS)-guided drainage of a perirectal abscess in a 62-year-old patient with Crohn's disease using a lumen apposing metal stent (LAMS). Visualisation of the large abscess (between the markers) with a rigid radial endorectal probe (a). Intervention is performed using a flexible longitudinal echoendoscope, starting with transmural puncture of the abscess with a 19 gauge aspiration needle (arrows, b). After aspiration of pus for microbiological examination, a 35 inch guidewire is inserted into the abscess, the transmural access route is dilated using a diathermic ring knife, and a fully covered LAMS is deployed under fluoroscopic and EUS control (c,d). Endoscopic and radiological view of the deployed stent with incomplete deployment in the area of the transmural access (e,f).